PMD CAMERA- AND HAND-EYE-CALIBRATION FOR ON-ORBIT SERVICING TEST SCENARIOS ON THE GROUND

Ksenia Klionovska[(1)], Heike Benninghoff[(1)], Klaus H. Strobl[(1)]
[(1)]German Aerospace Center (DLR), Münchener Str. 20, 82234 Wessling, Germany
Email: Ksenia.Klionovska@dlr.de

ABSTRACT

In this paper we present the ability to intrinsically and extrinsically calibrate a Time-of-Flight sensor, namely, a Photonic Mixer Device (PMD) camera, using the DLR CalDe and DLR CalLab camera calibration toolbox. This camera is intended as a visual sensor for pose estimation in the close rendezvous phase during future On-Orbit servicing. In order to test and verify the pose estimation algorithms on the ground, we conduct different rendezvous scenarios using the European Proximity Operation Simulator. It is necessary to accurately know intrinsic parameters like the focal length, the principal point, and the distortion parameters, as well as the extrinsic parameters, i.e., the position and orientation of the PMD camera relating to the mounting board, whenever it is fixed on the robot and involved in the process of target pose estimation. In this work we differentiate from state-of-the-art approaches for the calibration of PMD cameras in this context by making use of the motion of the mounting robotic manipulator alone, i.e., without the need for accurate positioning of the target calibration plate by a second robotic manipulator.

1. INTRODUCTION

Since the beginnings of outer space exploration, tremendous amount of waste rocket bodies, inactive satellites, and other fragmentation debris have been left on orbit. These objects represent a hazard to operative satellites, which in turn could lead to further increase of space debris. To overcome this problem, we conduct research in the simulation of On-Orbit Servicing scenarios on the ground, namely the Autonomous Rendezvous and Docking (RvD) setup with a vision unit, such as a Photonic Mixer Device (PMD) camera. The planned OOS activities include refueling, providing repairs, upgrading software and hardware of the satellite, and also deorbiting the satellite from the operative orbit [1]. We consider the following scenario: the visually guided robotic system, as a chaser, autonomously approaches the target, captures it (e.g. with a robotic arm) or docks on it and performs the necessary servicing tasks. The autonomous RvD approach uses only image information about the uncooperative target in order to estimate its pose (position and orientation) [2] with a consistent guidance of the robotic system approach the target [3].
Usually, vision systems for the autonomous RvD in space are specified by the requirements of the operation. In general, the application of one or the other sensor depends on the relative position between the chaser and the target, e.g. optical sensors for far, middle, and close range. About one decade ago a new type of the ranging systems such as Photonic Mixer Device camera became available [2, 4]. This depth sensor can measure the distance to the target on every pixel of a sensor chip. We investigate the features and benefits of the usage of a PMD sensor for pose estimation of the target satellite during close-range approach (from 25 m to 1 m).

1.2. EPOS facility

The simulation activity is a crucially important part and in most cases mandatory as a pre-step for the planned missions. The European Proximity Operation Simulator (EPOS 2.0) [5], located at the German Space Operations Center (GSOC), German Aerospace Center (DLR), is used as a ground-based hardware-in-the-loop (HIL) testbed for simulation of RvD operations. Via the presented EPOS setup, see Fig.1, the usability, reliability and safety of the developed guidance, navigation and control (GNC) system, hardware sensors (cameras or lasers) or docking tools [5] can be tested.
The EPOS facility consists of 2 standard 6 Degrees-of-Freedom (DOF) industrial robots.

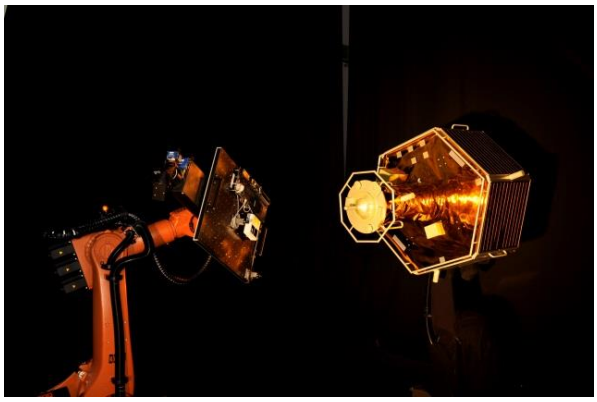

Figure 1. Two industrial robots of the EPOS facility

The Robot 1 (left on the Fig.1) is a KUKA KR100HA, which is mounted on a linear rail of 25*m* length and can be moved on along it in order to simulate an approach of the active satellite (chaser) to the passive one (target). The Robot 2 (right on the Fig.1), namely KUKA KR240-2, is fixed at the end of the rail system. Each robot has a breadboard attached to the flange, which can be used as a mounting board for the satellite mockups and RvD visual sensors.

1.3. Prerequisites to the camera calibration

By simulating the autonomous approach using the EPOS facility, the visual sensors (individually or by fusion of several sensors) and the developed pose

estimation algorithms can be tested. An accurately calibrated visual camera is a prerequisite in order to extract the information from 2D images and process it for the pose estimation of the target. Likewise usual mono- or stereo cameras, the PMD camera is required to be calibrated. In this paper we consider the camera calibration process as an estimation of the camera model (intrinsic calibration) and position and orientation of the PMD sensor frame in the camera housing (extrinsic calibration) with respect to (w.r.t.) the breadboard of the Robot 1.

1.3. Overview of calibration techniques

The well-known calibration toolboxes, such as Camera Calibration with OpenCV [12] or Camera Calibration Toolbox (CCT) for Matlab [11], are available in a public domain for estimation of the intrinsic and absolute extrinsic camera parameters. In the work of T. Tzschichholz [6], the author already calibrated the PMD sensor for using it with the EPOS facility. In his work, the CCT for Matlab is applied in order to estimate the intrinsic and absolute extrinsic parameters of the PMD camera. The transformation between the pose of the PMD camera and the Tool Center Point (TCP) of the robot's breadboard was determined by involving the knowledge about the relative position and orientation of the other robot in the chain of transformations.
The DLR CalDe and DLR CalLab calibration toolbox [7] is proposed in the present work as an alternative for the above mentioned methods. This calibration toolbox contains the well-known method of Zhang, Sturm and Maybank [9, 10] for the intrinsic calibration and the hand-eye calibration technique [19] for the extrinsic camera parameters. Critically, this toolbox does not require for the camera to perceive the whole calibration pattern in every image, which on the one hand is convenient for automated acquisition of images and on the other increases the accuracy of lens distortion estimation since features are more evenly spread in the images. Using the proposed toolbox we simplify the calibration procedures by working only with the robot, on which the camera is mounted. As far as we know, this is the first time that the designed setup for HIL for OOS Operations has been calibrated for such purposes.

2. VISION BASED NAVIGATION SYSTEM WITH PMD CAMERA

Vision based navigation is one of the proposed approaches in OOS missions for estimating the relative motion of the uncooperative target. To the best of our knowledge, the PMD camera has never been used in space application so far. Consequently, it is of great interest to conduct the image processing with this type of optical sensor on the ground in order to reveal its suitability for motion estimation in the close rendezvous phase.

Since the appearance and up to these days, the PMD technologies have been improved in terms of the resolution of the PMD chip (it has enhanced up to 352x288 pixels), measurement accuracy, and also robustness to the working condition. In this work we use a DLR-Argos3D - P320 camera, highlighted on the Fig.2 with a red frame. This camera contains two types of sensors: a 2D CMOS sensor and a 3D PMD sensor with resolution of 352x287 pixels and a field of view 28.91x23.45 degrees. As we are interested only in the PMD sensor, the details concerning the 2D sensor will be omitted.

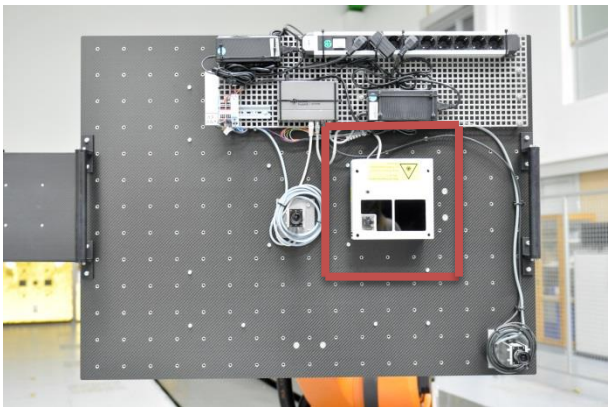

Figure 2. DLR-Argos3D - P320 camera fixed on the breadboard in the EPOS laboratory

2.1. PMD camera working principle

The depth measurement principle of the PMD sensor inside of the DLR-Argos3D - P320 camera is based on the computed phase shift of a periodical modulated signal. The phase shift is measured between the emitted modulated light from 12 IR-flash LEDs integrated in the camera and the reflected light from the observed surface. The distance to the target can be calculated pixelwise as follows:

$$d = \frac{c\varphi}{4\pi f_{mod}}. \qquad (1)$$

In the equation 1, c is the speed of light $c = 3 \times 10^8$ m/s, φ is the measured phase shift and f_{mod} is the modulation frequency of the emitted signal.
Beside the distance information, usually a PMD sensor provides additional amplitude values by the same pixel array at the same time. The amplitude image corresponds to the amount of the returning active light and presents the quality of the measurements [13]. The higher amplitude value of a pixel, the more reliable is the distance value. Since we get the amplitude image of the scene, we can handle it as a gray-scaled image described by the pinhole camera model [14]. Considering this fact, we can perform the calibration of the PMD sensor by the same techniques used for the

calibration of the standard cameras and structured light depth cameras.

2.2. Perspective Camera Model

As we treat the amplitude image as a gray-scaled image, we can characterize the relationship between the coordinates of a 3D point of the scene and its projection onto the image plane (depth grid in our case) by the pinhole camera model [18].
A 2D point of the image plane is denoted as $m = [u, v]^T$ and a 3D point is expressed as $M = [X, Y, Z]^T$[9]. In homogeneous coordinates the vectors are presented by $\tilde{m} = [u, v, 1]^T$ and $\tilde{M} = [X, Y, Z, 1]^T$. The projection of a 3D point *M* onto the image plane is described by

$$s\tilde{m} = A[R\ t]\tilde{M}, \qquad (2)$$

where *s* is an arbitrary scale factor, [*R*, *t*] are extrinsic parameters in form of rotation and translation, and *A* is a camera calibration matrix [9]. The calibration matrix *A* is presented by

$$A = \begin{bmatrix} \alpha & \gamma & u_x \\ 0 & \beta & v_y \\ 0 & 0 & 1 \end{bmatrix} \qquad (3)$$

and includes the following parameters: focal lengths α and β, coordinates of the principal point (u_0, v_0), and a skew factor γ between x and y axis.

3. DLR CALDE AND DLR CALLAB CALIBRATION TOOLBOX

3.1. Intrinsic camera calibration

The proposed calibration toolbox outlines the intrinsic camera calibration approach, which was made by Zhang [9] and Sturm and Maybank [10]. They presented a closed-form solution by linear least-squares techniques for the initialization of the nonlinear optimization [15]. For the accurate camera calibration, one has to detect and identify the visible control point (corners) of the planar calibration pattern ${}_0x_i = [x_i\ y_i\ z_i]^T$ perspectively projected onto the image frame in every image $n \in \{1, \dots, N\}$ as ${}_n\tilde{m}_i$. These measured projections are corrupted with noise and are compared with the estimated ones ${}_n\hat{m}_i = [\ {}_nu_i,\ {}_nv_i, 1]^T$ using the Euclidean decomposition of the perspective projection matrix $P = A\ {}_cT^0$ as follows:

$$s\hat{m} = A\ {}_cT^0\ {}_0x = \begin{bmatrix} \alpha & \gamma & u_x \\ 0 & \beta & v_y \\ 0 & 0 & 1 \end{bmatrix} [r_1\ r_2\ t] \begin{bmatrix} x \\ y \\ 1 \end{bmatrix} \qquad (4)$$

where *s* is an arbitrary scale factor, ${}_cT^0$ the rigid body transformation from the camera frame to the object/world frame in the image *n*, and *A* is a camera calibration matrix. We assume that the model plane is on z=0, so that r_3 disappears and the homography between the calibration plane and the image simplifies to the linear projective transformation $H = [\ h_1\ h_2\ h_3\ ]$. The *N* homographies $\hat{H}_n$ between image projections ${}_n\tilde{m}_i$ and pattern features ${}_0x_i$ can be estimated. We have $\hat{H} = \lambda A[r_1\ r_2 t]$, where λ is an arbitrary scalar. Knowing that r_1 and r_2 are orthonormal, we get the following equations:

$$\left.\begin{aligned} (A^{-1}h_1)^T \cdot (A^{-1}h_2) &= 0 \\ (A^{-1}h_1)^T \cdot (A^{-1}h_1) &= (A^{-1}h_2)^T \cdot (A^{-1}h_2) \end{aligned}\right\}. \qquad (5)$$

Note that $\omega_\infty = A^{-T}A^{-1}$ describes the image of the absolute conic and the system of equations transforms to:

$$\left.\begin{aligned} {h_1}^T \omega_\infty h_2 &= 0 \\ {h_1}^T \omega_\infty h_2 &= {h_2}^T \omega_\infty h_2 \end{aligned}\right\}. \qquad (6)$$

These two equations are taken for every image *N*, leading to *2N* constrains for 5 intrinsic unknowns. They can be solved by using a least-square criterion, if at least three different views ($N \geq 3$) are available.
Once the camera calibration matrix is known, the extrinsic parameters for image *N* are ready to compute:

$$\begin{aligned} r_1 &= 1/s \cdot A^{-1} \cdot h_1 \\ r_2 &= 1/s \cdot A^{-1} \cdot h_2 \\ r_3 &= r_1 \times r_2 \\ t &= 1/s \cdot A^{-1} \cdot h_3 \\ s &= \|A^{-1} \cdot h_1\| = \|A^{-1} \cdot h_2\|\,. \end{aligned} \qquad (7)$$

3.2. Lens distortion

Up to now we did not consider the lens distortion of the camera, which significantly spoils the linear projective formulation of the camera. Usually the lens systems of the real cameras are affected by the nonlinear aberrations. These distortions are mainly caused as a symmetric displacement along the radial direction from the principal point [17]. Taking in consideration the radial distortion, the pinhole camera model is extended by an additional distortion model, which is described by the polynomial formulation:

$$\delta_r(\rho) = k_1\rho^3 + k_2\rho^5 + k_3\rho^7 + O(\rho^9) \qquad (8)$$

where ρ is the radial distance from the center of radial distortion to the expected normalized projection and k_1, k_2, k_3 are the coefficients of the radial distortion.
The optimal parameters estimation can be obtained by minimizing the following functional:

$$\hat{\Omega}_* = \arg\min \sum_{n=1}^{N} \sum_i \left\| {}_n\tilde{m}_i - {}_n^d\hat{m}_i(\hat{\Omega}, \boldsymbol{\Upsilon}\ ({}_0x_i)) \right\|^2 \quad (9)$$

where ${}_n^d\hat{m}_i$ are the distorted projections of the control points ${}_0x_i$ expected in the image frame; Ω is a set of calibration parameters to be estimated (intrinsic, distortion, and absolute extrinsic); $\boldsymbol{\Upsilon}$ are the system models, which include the camera and lens distortion models as well as the calibration object model (e.g. ${}_0x_i$) [9, 15,20].

3.3. Extrinsic camera calibration

Whenever the sensor is mounted on a robot, it is important to define the rigid-body transformation of the PMD sensor (eye) frame S_S relating to the TCP frame of the Robot 1 (hand) S_R [16]. This problem is referred as a hand-eye calibration. Thanks to this transformation ${}_ST^R$ we are able to map the sensor's measurements into the robot frame for further processing.

The common solution of the hand-eye camera calibration is formulated as: move the hand of the robot and observe/perceive the movement of the eye. The mathematical representation is:

$$AX = ZB \quad (10)$$

Here X is a desired homogeneous transformation relating the pose of the camera/sensor frame to the pose of the TCP frame of the robot ${}_ST^R$; A is a homogeneous transformation relating the pose of the object/world frame of the calibration object to the pose of the camera/sensor frame, which we obtain during the intrinsic calibration phase [9]; Z is the unknown (yet irrelevant) transformation between the object/world reference frame and the base frame of the robot; and B is a homogeneous transformation relating the base frame of the robot and the pose of the TCP frame. At least $n=3$ stations are required in order to uniquely determine the transformation ${}_ST^R$ [16]. In a nutshell, the rigid body transformation X can be retrieved by minimizing the discrepancies between A and B.

4. PMD CAMERA CALIBRATION PROCESS

The intrinsic and hand-eye calibration techniques, which were described previously, are state-of-the art for monocular and stereo cameras. In this section we show a feasible use of them for the calibration of the PMD sensor within the DLR-Argos3D - P320 camera by using the DLR CalDe and DLR CalLab calibration toolbox. The common brief tutorial how to use this calibration toolbox can be found in [7].

We used a rigid checkerboard pattern, which is defined by n_x=18 and n_y=12 squares, where the dimension of every square is specified as $u_x \times u_y \approx 30 \times 30\,mm$. Inaccuracies during the manufacture or printing of the pattern inherit regularly in the checkerboard and not every rectangle has the exactly mentioned size. Therefore, according to [16], we recalculated the estimated values of the rectangles with the aid of an electronic ruler and acquired the actual size as $29.91 \times 29.95\,mm$. The calibration pattern was fixed in front of the robot with the mounted camera on the breadboard plane of the Robot 1, see Fig. 3.

Figure 3. Setup of the calibration pattern and the camera

The Robot 1 has been moved to 8 different positions in order to image the calibration pattern. Only the amplitude images of the PMD sensor were used in place of color images of the standard cameras. On Fig. 4 eight pictures (2 images from each side) of the amplitude channel are shown.

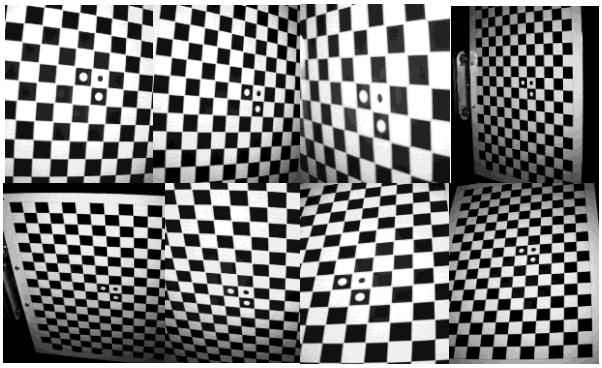

Figure 4. Calibration images from the PMD sensor

There was no need to get the whole pattern plate in the image, but getting the sharp images is one of the prerequisites for accurate calibration. Due to the limitation in the rotation of the robot axes, it is difficult to collect sharp images from above and below. During the acquisition of the calibration images, the robot pose w.r.t. the Global Laboratory Coordinate (GLC) frame was stored for every amplitude image respectively. On Fig. 5 the orientation of the X, Y, and Z axes is presented.

The information about the robot pose is required in order to calculate the hand-eye-calibration. Having completed the image collection, we started DLR CalDe

in order to localize landmarks and corners on the chessboard with sub-pixel accuracy.

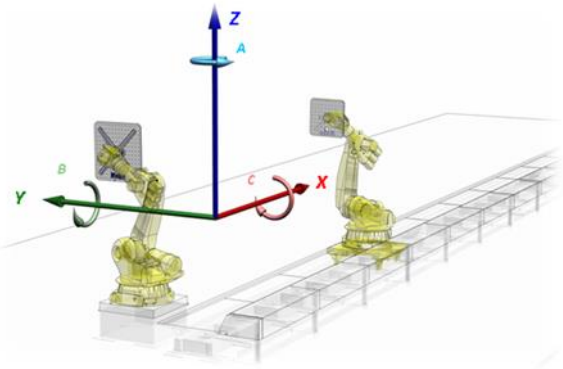

Figure 5. Global Laboratory Coordinate System

It is important to fill up correctly the chessboard parameters on the right side of the main window of the DLR CalDe toolbox (Fig.6) in order to let the program detect the corner points precisely and automatically. On the Fig.6 one can observe the image with the accurately detected corners of the calibration plate. The recognized points were saved and further used as an initial basis in the DLR CalLab toolbox.

To get the intrinsic and extrinsic parameters we run the calibration toolbox DLR CalLab. The user can choose and set numerical optimization algorithms and a variety of estimation methods. The calibration process is fully automatic and performed in one-button mode. On Fig.7 the main window of the DLR CalLab application with the output results is depicted.

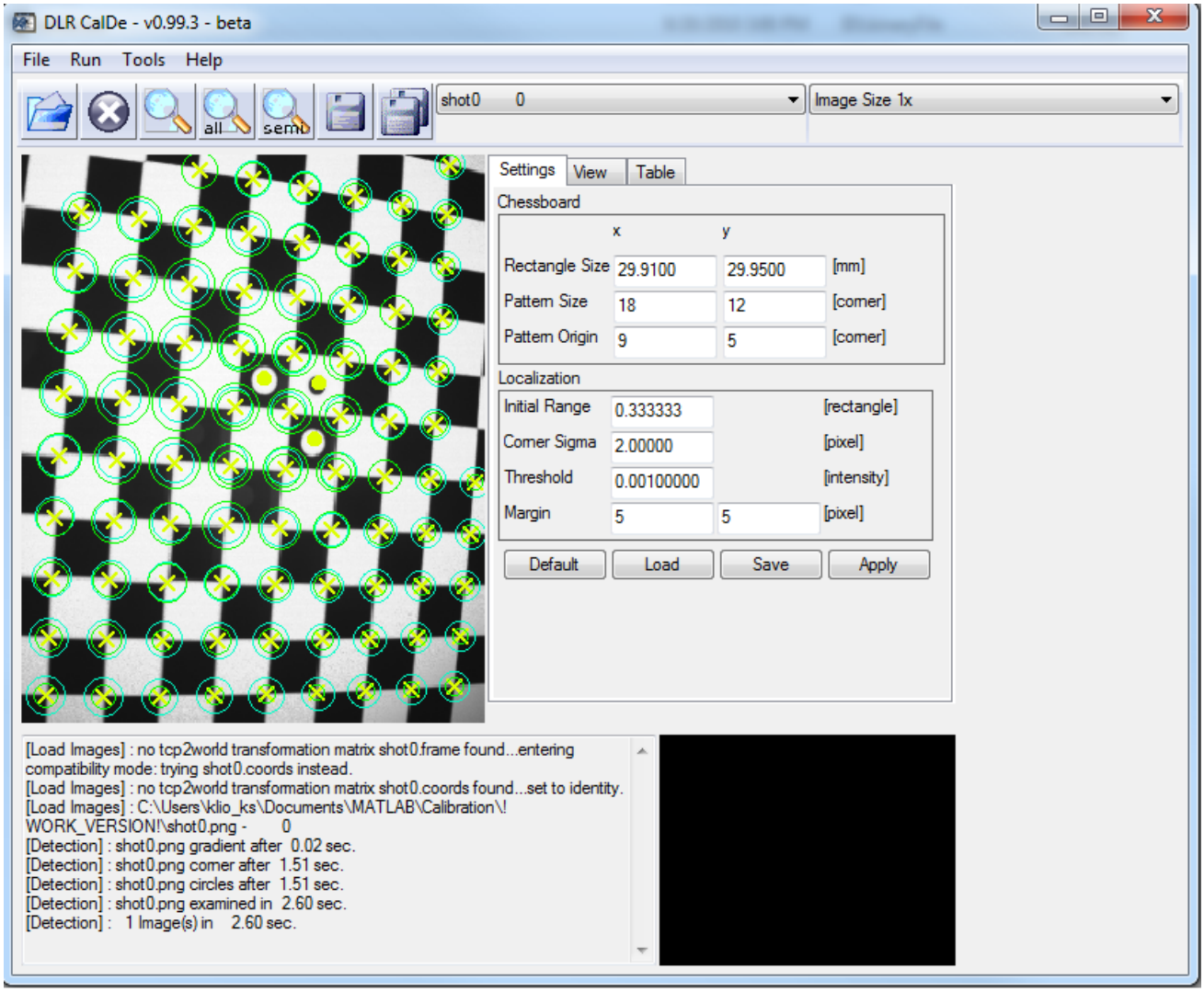

Figure 6. DLR CalDe detects the corner points in the image

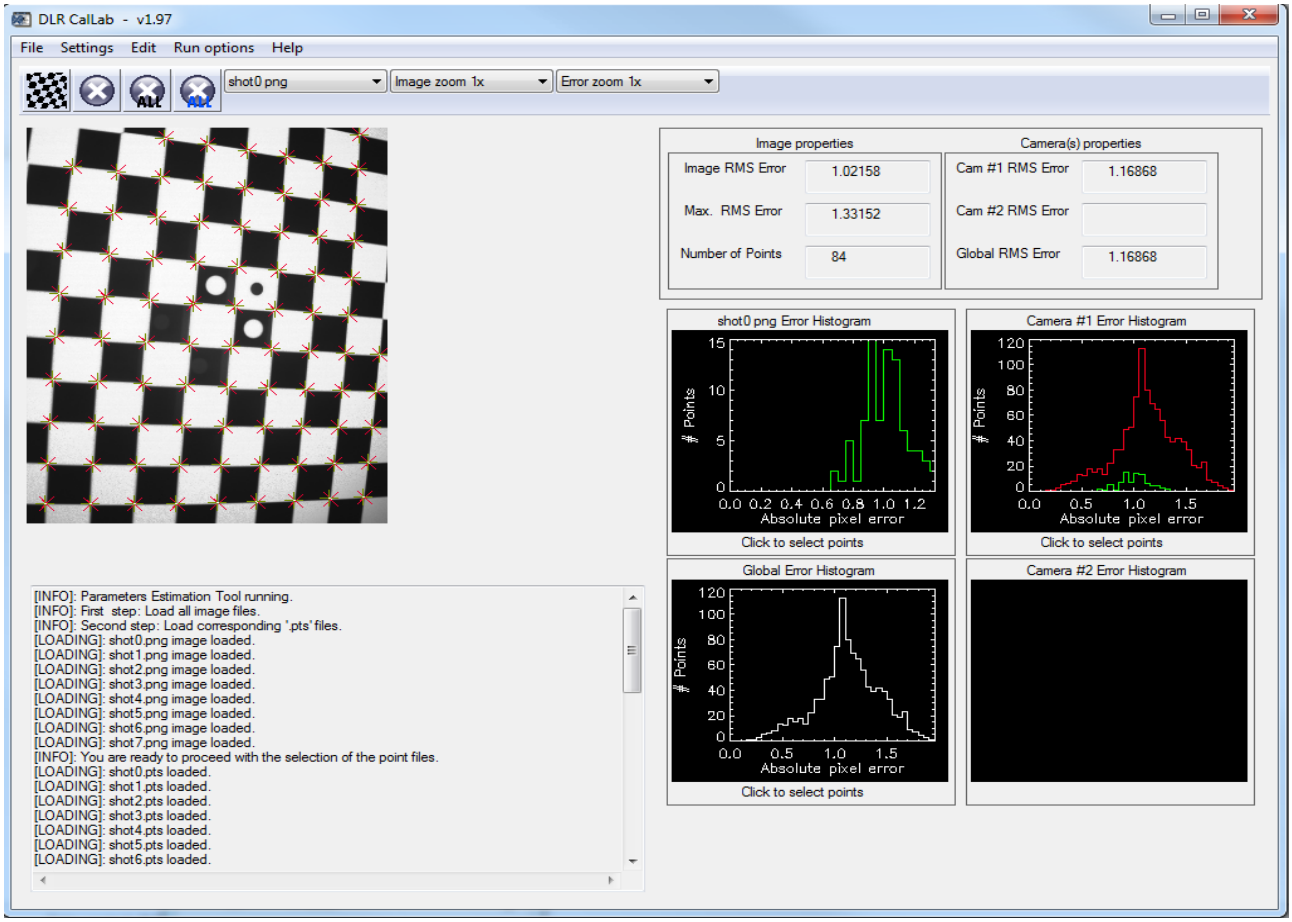

Figure 7. DLR CalLab dialog window with output results

4.1. Numerical results

By running the calibration process we got the file with the following results for the PMD sensor inside of the DLR-Argos3D - P320 camera:

a) Calibration matrix is presented as:

$$A = \begin{bmatrix} 705.748 & 0.581 & 143.578 \\ 0 & 704.082 & 184.228 \\ 0 & 0 & 1 \end{bmatrix}$$

b) Distortion coefficients k_1=-0.4973 and $k_2 = 0.3251$.

c) The transformation matrix ${}_S T^R$, which describes the pose of the sensor inside of the DLR-Argos3D - P320 camera relating to the chosen TCP point of the Robot 1:

$${}_S T^R = \begin{bmatrix} 0.9999 & -0.0043 & -0.0022 & -42.874 \\ 0.0043 & 0.9999 & 0.0134 & -186.912 \\ 0.0021 & -0.0134 & 0.9999 & 145.847 \end{bmatrix}$$

d) Root mean square (RMS) error after intrinsic calibration is 0.177 pixels; after extrinsic calibration it reads 1.192 pixels or 0.21° and 2.92 mm. Note that we are not explicitly minimizing the former pixel RMS error but the latter position and orientational errors of the robot manipulator as detailed in [16]. In doing so, the reprojection error in pixels might be slightly worse, but the estimation of the hand-eye transformation is optimal since the actual, biggest errors in the system (viz. the positioning errors of the robotic manipulator) are being minimized.

5. CONCLUSION

In this paper we showed how the PMD sensor can be precisely calibrated before integrating it in HIL simulations of the OOS scenarios on the ground. Contrary to state-of-the-art methods, in doing so we only made use of the motion readings of the robot where the camera is mounted and not of the motion of the external calibration object (potentially mounted on a second manipulator robot). In order to obtain the intrinsic and hand-eye calibration parameters of the PMD sensor, we used the DLR CalDe and DLR CalLab calibration toolbox, which includes state-of-the art calibration techniques for regular cameras and was not originally developed for the PMD sensors.

6. REFERENCES

1.Andrieu, M. (2004). *Space 2030: Exploring the Future of Space Applications*. Organization for Economic Cooperation and Development OECD, pp.126-127.

2.Klionovska, K. & Benninghoff, H. (2017). *Initial pose estimation using PMD sensor during the rendezvous phase in on-orbit servicing missions*. 27th AAS/AIAA Space Flight Mechanics Meeting, Texas, USA.

3.Qureshi, F. & Terzopoulos, D. (2008). *Intelligent perception and control for space robotics: autonomous satellite rendezvous and docking*. Journal of Machine Vision Application 19(3), 141-161.

4.Ringbeck,T. & Hagebeuker, B. (2007). *A 3D Time of Flight Camera for object detection*. Oprtical 3-D Measurement Techniques, ETH Zürich.

5.Benninghoff, H. et.al. (2017). European Proximity Operations Simulator 2.0 (EPOS) - A Robotic-Based Rendezvous and Docking Simulator. Journal of large-scale research facilities. 3, A107.

6.Tzschichholz, T. (2014). *Relative pose estimation of known ridged objects using a novel approach to high-level PMD-/CCD- sensor data fusion with regard to applications in space*. Dissertation, University of Würzburg, Germany.

7.Strobl K. H. et al. *DLR CalDe and DLR CalLab*. Institute of Robotics and Mechatronics, German Aerospace Center (DLR), Oberpfaffenhofen, http://www.robotic.dlr.de/callab/

8.Hartley R. I. & Zisserman A.(2004). *Multiple View Geometry in Computer Vision*. Cambridge University Press, ISBN: 0521540518, second edition.

9.Zhang, Z. (2000). *A Flexible new Technique for Camera Calibration*. IEEE Transactions on Pattern Analysis and Machine Intelligence , vol. 22, no. 11, pp. 1330–1334.

10.Sturm P. F. & Maybank, S. J. (1999). *On Plane-Based Camera Calibration: A General Algorithm, Singularities, Applications*. in Proc. of the IEEE Conf. on Comp. Vision and Pattern Recogition CVPR, pp. 432–437, FortCollins, USA.

11.Bouguet, J. Y. *Camera calibration toolbox for Matlab*. ttp://www.vision.caltech.edu/bouguetj/

12.*Camera calibration with OpenCV*. http://docs.opencv.org/2.4/doc/tutorials/calib3d/camera_calibration/camera_calibration.html

13.Lefloch, D. et al. (2013). *Technical foundation and Calibration Methods for Time-of-Flight Cameras*. Time-of-Flight and Depth Imaging. Sensors, Algorithms, and Applications, pp.3-24.

14. Fuchs, S. & Hirzinger G. (2008). *Extrinsic and depth calibration of ToF-cameras*. in Proc. 22nd IEEE Conf. Computer Vision Pattern Recognition, vol. 1-12, Anchorage, pp. 3777–3782.

15.Strobl, K. H. & Hirzinger, G. (2008). *More Accurate Camera and Hand-Eye Calibrations with Unknown Grid Pattern Dimensions*. Proceedings of the IEEE International Conference on Robotics and Automation (ICRA 2008), Pasadena, California, USA, pp. 1398-1405.

16.Strobl, K. H. & Hirzinger, G. (2006). *Optimal Hand-Eye Calibration*. Proceedings of the IEEE/RSJ International Conference on Intelligent Robots and Systems, Beijing, China, pp. 4647-4653.

17.Lindner, M. (2010). *Calibration and Real-Time Processing of Time-of-Flight Range Data*. Dissertation. University of Siegen. Germany.

18.Ma Y. et al. (2004). *An Invitation to 3D Vision*. *Springer*.

19.Tsai, R., Y. & Lenz, R., K. (1989). *A New Technique for Fully Autonomous and Efficient 3D Robotics Hand/eye Calibration*. IEEE Trans. on Robotics and Automation, vol. 5, no. 3, pp. 345–358.

20.Strobl, K., H. (2014). *A flexible approach to close-range 3-D modeling*. PhD thesis, Institute for Data Processing, Fakultät für Elektrotechnik und Informationstechnik, Technische Universität München, Munich, Germany.